BM@N experiment
JINR, October 2, 2024

Analysis Note

Study of neutron emission from target spectators in ^{124}Xe + CsI collisions at 3.8 *A* GeV

Nikita Lashmanov[1], Vladimir Yurevich[2], Sergey Sedykh, Viktor Rogov, Sergey Sergeev, Vladimir Tikhomirov, Vitaliy Azorskiy, Alexandre Timoshenko, Valio Velichkov

Joint Institute for Nuclear Research, Dubna, Russia

The results on neutron energy spectra were obtained in collisions of ^{124}Xe nuclei with a CsI target at a beam energy of 3.8 *A* GeV in the last BM@N run. The measurement was performed with a compact TOF neutron spectrometer in wide energy range up to 200 MeV for emission angles of 95°, 110° and 121° that corresponds to the neutrons emitted in the decay of spectators of the target nuclei. The obtained neutron energy spectra are well reproduced by phenomenological model of three moving sources. In the energy region below 20 MeV, the angular distribution is isotropic. It indicates that the velocity of this neutron source is close to zero. A comparison with prediction of DCM-QGSM-SMM code shows need of further code development by adding neutron evaporation process for description of low energy part of neutron spectra.

1. E-mail: lashmanov@jinr.ru
2. E-mail: yurevich@jinr.ru

Contents

1. Introduction

In nuclear collisions at intermediate and high energies, a large number of neutrons are emitted, which carry away a significant part of the energy of the incident nucleus. Experimental data that allow obtaining new information about the process of formation of free neutrons in the nucleus - nuclear collisions are of great interest for understanding the mechanism of evolution of the resulting highly excited nuclear system and the further development of theoretical models.

However, despite the importance of these data, the number of such experiments remains very limited, which is explained by the methodological complexity of conducting neutron measurements. To date, the bulk of studies have been performed on heavy ion beams of the Bevalac/LBL [1 - 3], SIS/GSI [4 - 7] and HIMAC/NIRS [8, 9] accelerators in the intermediate energy range from 150 to 1000 *A* MeV, in which the energy and angular distributions of neutrons were studied. In the higher energy region, only a few experiments have been performed with beams of 2 *A* GeV C nuclei at JINR [10], 10.6 *A* GeV Au at BNL [11], 158 *A* GeV Pb at SPS/CERN [12] and for Pb + Pb collisions at the LHC collider at $(s_{NN})^{1/2}$ = 5.02 TeV [13]. In the last two cases, the multiplicity of neutrons from the decay of the beam spectator nucleus was studied as a function of the collision centrality.

It should be noted that a detailed study of neutron emission by a spectator nucleus requires an experiment with a fixed target, in which the energy spectrum of neutrons is measured at large angles to the beam direction in a wide energy range from units to hundreds of MeV from the decay of target nuclear spectators. Such measurements can be implemented by the time-of-flight method with neutron detectors based on organic scintillators. The implementation of the TOF method requires the fulfillment of a number of special conditions and, as a rule, the use of large flight distances of several meters or more [1]. The developed compact time-of-flight spectrometer with a record high time resolution (100 ns) and a flight distance of several tens of centimeters is designed to measure neutron spectra in the energy range from 1 to 200 MeV and has a number of significant advantages compared to traditional (room scale) TOF spectrometers. Due to its small size (table scale), it allows to significantly increase the rate of collecting event statistics with a small contribution of secondary neutron background.

The compact TOF neutron spectrometer has been implemented into the BM@N setup [14] on the extracted beam of nuclei with an energy of up to 4 *A* GeV from the Nuclotron accelerator at the LHEP JINR.

The aim of the developed TOF spectrometer is to measure the double differential neutron production cross sections for neutrons emitted in decay of target nuclear spectators in nucleus – nucleus collisions. The performance of the spectrometer was studied in the BM@N run 2022 – 2023 with the beam of 3.8 *A* GeV ^{124}Xe ions bombarded CsI target. In this note we report the characteristics of the spectrometer and analysis the first results.

2. The compact TOF neutron spectrometer

Spectrometer description

The main requirements for the neutron spectrometer being developed are:

1. the time resolution of the spectrometer, reduced to a flight base of 1 m, should be no worse than $\sigma_t \approx 0.5$ ns,
2. effective discrimination of events caused by charged particles and gamma quanta,
3. small contribution from background neutrons,
4. the time for collecting the required statistics of neutron events should not exceed several days,
5. the ability to operate in a strong magnetic field of the large BM@N analyzing magnet,
6. event-by-event data recording together with data from other BM@N detectors.

The required time resolution is achieved by using a start detector with a picosecond time resolution and neutron detectors (ND) based on small-volume stilbene crystals coupled with SiPM silicon photomultipliers, as well as by using fast electronics developed and manufactured at LHEP JINR.

Discrimination of events caused by charged particles is performed by placing veto detectors (VD) with 5-mm plastic scintillators in front of the neutron detectors. For effective suppression of the gamma-quantum background, the method of separating events caused by neutrons and gamma-quanta by the pulse shape in stilbene (PSD method) is used.

To meet points 3 and 4 of the above requirements in the experimental conditions of the BM@N setup, it is necessary to use flight distances of several tens of centimeters, taking into account the placement of the spectrometer detectors in a limited space inside the BM@N magnet, as well as the high intensity of the nuclear beam of ~10^6 nuclei per 2 – 3 s spill. To suppress the background caused by the interaction of the beam nuclei with air, all beam detectors and the target are located inside the vacuum beam tube.

The spectrometer's ability to operate in a magnetic field of B = 0.9 T of the BM@N magnet is achieved by using SiPMs instead of photomultipliers in the ND and VD detectors.

An important feature of the spectrometer is the implementation of event-by-event recording of information from the spectrometer detectors by digitizing it, which significantly expands the possibilities of data analysis together with data from other detectors of the BM@N facility. For example, this approach allows studying the dependence of neutron emission on the centrality of nucleus-nucleus collisions.

The layout of the neutron spectrometer in the BM@N experimental area is shown in Fig. 1.

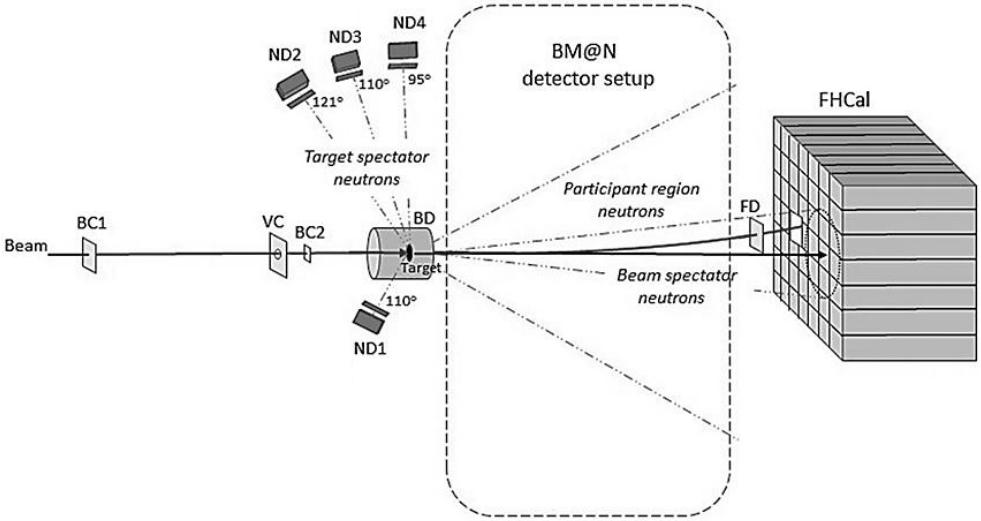

Fig. 1. Schematic view of the neutron spectrometer in the BM@N experiment channel: ND1 – ND4 – neutron detectors, BC1, VC, BC2, FD – beam scintillation detectors, BD – multichannel scintillation detector, FHCal – forward hadron calorimeter.

The starting detector is a BC2 beam detector with a 150- μm thick BC400B plastic scintillator, viewed by two XPM85112 microchannel plate photomultipliers (Photonis). The detector's intrinsic time resolution is 40 ps. The neutron detectors generate a stop pulse.

Four neutron detectors were used in the studies, which were located at an angle to the beam direction of 110° at a distance of 20 cm from the target (detector ND1) and at angles of 121°, 110° and 95° at a distance of 30 cm from the target (detectors ND2 – ND4). The aim of detector ND1 is to improve reliability of results obtained in the low energy range, below 15 MeV.

The BM@N setup interaction trigger is used as a trigger for the nucleus-nucleus interaction in the target, using pulses from the fast scintillation beam detectors BC1, VC, BC2,

FD and the multichannel detector BD, inside which the target is located. These pulses are fed to the inputs of a specialized T0U module [14] with programmable logic, which generates an interaction trigger signal when the following conditions are met:

1. the presence of pulses with an amplitude corresponding to the incident ion in the beam scintillation detectors BC1 and BC2(T0), located in front of the target,
2. the absence of a pulse in the scintillation veto counter VC with an aperture forming a beam spot on the target,
3. the absence of a pulse with an amplitude corresponding to the incident ion in the scintillation detector of nuclear fragments FD, located at a distance of 7.8 m behind the target,
4. the number of pulses from the scintillation strips of the detector BD (Barrel Detector), which has the form of a cylinder and is located around the target, exceeds the set threshold value N_{th}.

Fulfilment of the first and second conditions forms a trigger on the incident ion, Beam Trigger (BT). And the logic of generating the interaction trigger, Interaction Trigger (IT), is written as

$$IT = BT * FD_{veto} * BD(N > N_{th}) . \quad (1)$$

The described event selection trigger cuts off a part of peripheral collisions with a large impact parameter. The average number of triggered channels of the BD detector increases when moving from peripheral to central collisions of nuclei. Therefore, increasing the threshold N_{th} means registering more central collisions.

Neutron detectors

The neutron detectors have a rectangular aluminum case, inside which there are two identical stilbene crystals in a standard package with a glass window. One ND1 detector with stilbene crystals of 30 mm in diameter and 10 mm in thickness and three ND2 – ND4 detectors with stilbene crystals of 25.4 mm in diameter and thickness were manufactured. Each stilbene was viewed by an assembly of four SiPMs) SensL 6×6 mm^2, J-ser., the pulses from which are fed to the front-end electronics (FEE) board. The fast output is used for time-of-flight measurements as a stop signal, and the slow output transmits the full pulse shape and is used to separate events caused by neutrons and gamma quanta by the pulse shape, which ensures significant background suppression in neutron measurements. The circuit and appearance of the detectors are shown in Fig. 2.

The VD veto detectors have a plastic scintillator 80×40×5 mm^3, viewed by two SiPMs.

Each arm of the spectrometer, consisting of a neutron detector with two stilbene crystals and a scintillation veto detector, had three independent particle registration channels.

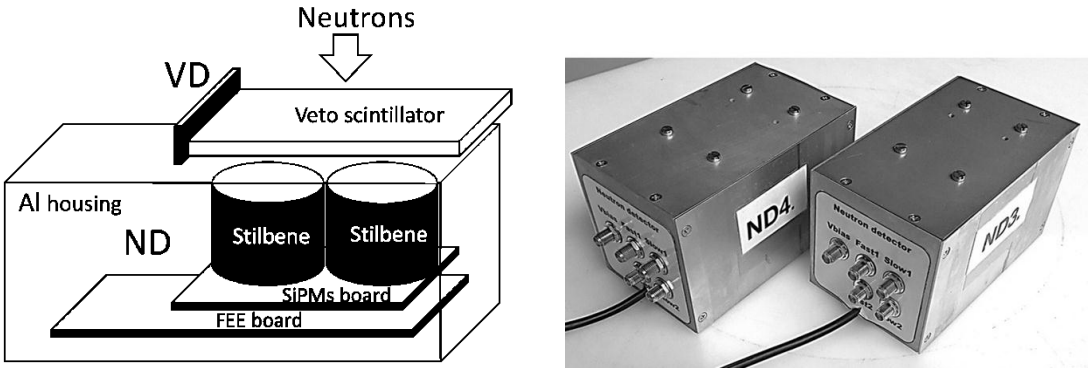

Fig. 2. A scheme and view of neutron detectors.

The neutron channel based on one stilbene includes a detecting assembly based on stilbene and four SiPMs, a Front-End electronics board and digitalization and data acquisition electronics.

The digitalization electronics module has two independent channels for converting and recording pulses generated by the Front-End electronics board. The analog fast pulse carries time information and is used as a stop pulse in time-of-flight measurements. The other full pulse is used in pulse shape analysis for gamma-quanta discrimination. The neutron channel diagram is shown in Fig. 3.

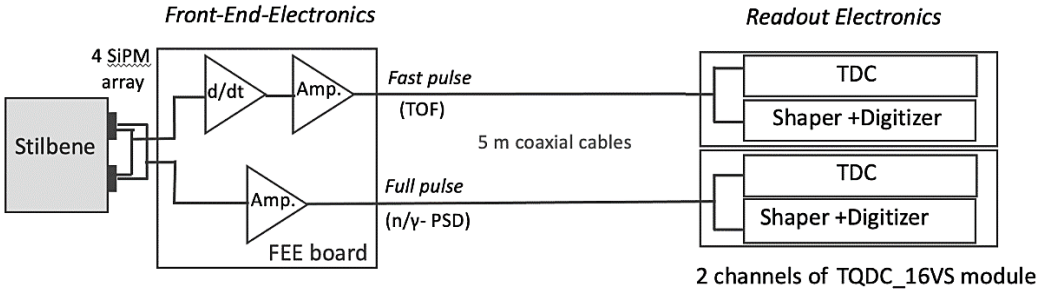

Fig. 3. A scheme of neutron channel.

To record events from neutron and veto detectors, electronic modules TQDC16VS [15] in the VME standard were used. These modules are part of the BM@N data acquisition system and perform digitization of time and shape of the input signal.

The TQDC16VS module contains 16 inputs for analog signals with an input pulse range of ±1 V; TDC, recording the arrival time of input pulses with a step of 25 ps and ADC, performing continuous digitization of the amplitude with a quantization resolution of 14 bits and a sampling frequency of 125 MHz. The module also has 4 programmable synchronization inputs/outputs (50 Ω LVTTL) and a data transfer interface over 1 or 10 Gb/s Ethernet.

Neutron detection efficiency

Neutron detection in organic scintillators occurs by their scattering on hydrogen nuclei with a cross-section of σ(np) [16, 17] with the transfer of part of the energy to the proton, as well as due to reactions on carbon nuclei with the formation of secondary charged particles with a cross-section of σ_{ch}, which was estimated as the difference between the cross-section of inelastic interaction [18, 19] and the cross-sections of the reactions (n,n'γ) [18] and (n,2n) [18, 20]. The dependence of the registration efficiency on the neutron energy for small-sized scintillators was calculated in the single-interaction approximation using the expression

$$\varepsilon = (1 - e^{-\Sigma h}) \left[\frac{\Sigma_H}{\Sigma} \left(1 - \frac{B_H}{E}\right) + \frac{\Sigma_C}{\Sigma} \left(1 - \frac{B_C}{E}\right) \right] , \qquad (2)$$

where

$$\Sigma = \Sigma_C + \Sigma_H = n_C \, \sigma_{ch}(nC) + n_H \, \sigma(np) \quad ,$$

$\sigma_{ch}(nC)$ is the cross-section for the formation of charged particles in reactions with carbon nuclei, σ(np) is the cross-section for elastic np-scattering, h – the thickness of stilbene, B_H – the threshold energy for recoil protons in *np*-scattering, B_C – the threshold energy in reactions with carbon nuclei.

In our case, the threshold energy of neutrons corresponds to the maximum energy of protons in elastic np-scattering. Its position is uniquely determined on the time scale of the neutron time-of-flight spectrum, and an analysis of the amplitude distribution at this point in the time scale allows one to find the threshold amplitude value. A good check for the correctness of the chosen threshold value is the decay of the direct neutron time-of-flight spectrum to zero at this point. The corresponding threshold energy value for alpha particles, used in the formula for calculating the efficiency, was calculated using the dependence of the stilbene light yield on the alpha particle energy taken from [21].

To test the method, the efficiency was calculated for various neutron detectors based on stilbene and NE213 with dimensions not exceeding 5 cm, for which measurement results are available [21 – 25].

The discrepancy between the calculated and experimental values does not exceed 10%, which demonstrates the applicability of this approach to assessing the efficiency of neutron detectors with thin organic scintillators in a wide energy range. As an example, Fig. 4 shows the calculated neutron detection efficiencies for the ND2 – ND4 detectors for detection thresholds of 0.5, 0.8, 1.0 and 2.5 MeV. The results of measurements [21] performed with stilbene of the same dimensions at threshold energies of 0.5 and 0.8 MeV are also given there.

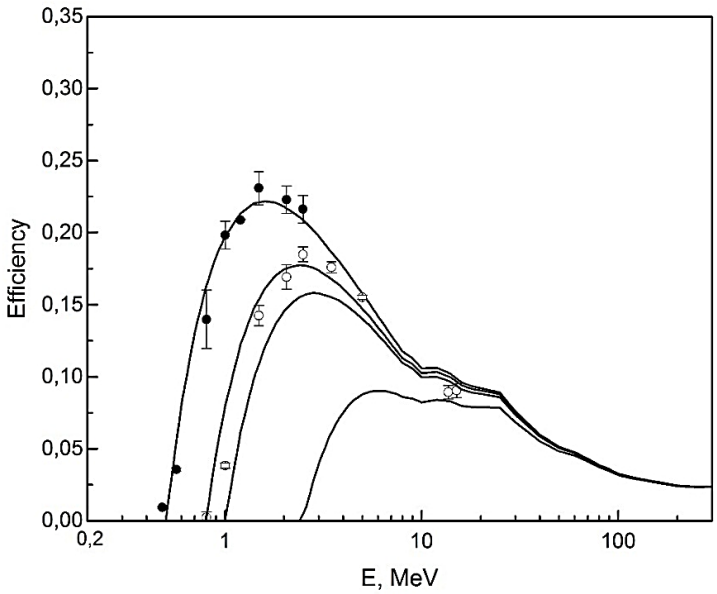

Fig. 4. Calculated efficiencies for neutron detectors ND2 – ND4 for registration thresholds of 0.5, 0.8, 1.0 and 2.5 MeV. The dots show the experimental results [21] for thresholds of 0.5 and 0.8 MeV.

3. Study of the spectrometer performance with Xe + CsI collisions

Data selection for analysis

The event selection for data processing was made with trigger CCT2 and B/A protection ± 1.8 μs for Xe-ion pulse in the BC1 detector. In this case the event statistics was reduced but we got clear reference result with minimal background and pulse shape distortion in the neutron detectors that is important for good n/γ- discrimination. As an example, in Table 1 a list of runs and event statistics obtained for the ND4 detector are shown. After the B/A protection only 23% of events were selected. In these collision events the ND4 detected gamma-rays in 1% events and neutrons in 0.16% events. As the result, 34103 neutron events were collected for analyses.

In final analysis the statistics will be increased by a factor of 3 by using another protection condition: BC1 pulse with B/A-protection ±250 ns and for interactions (BC1 * FD_{veto}) the protection interval of ±1.8 μs.

Table 1. A list of runs and event statistics obtained for the ND4 detector

	Run:	**Events**:
ND4 (93-runs)	7623, 7579, 7581, 7584, 7585, 7586, 7587, 7591, 7596, 7597, 7607, 7609, 7622, 7630, 7633, 7634, 7638, 7639, 7640, 7643, 7644, 7645, 7646, 7647, 7655, 7656, 7660 7662, 7663, 7664, 7665, 7666, 7668, 7669, 7670, 7671, 7673, 7674, 7675, 7681, 7682, 7684, 7685, 7687, 7689, 7690, 7692, 7693, 7717, 7718, 7721, 7723, 7724, 7725, 7726, 7727, 7728, 7729, 7730, 7732, 7733, 7734, 7737, 7751, 7753, 7761, 7762, 7763, 7764, 7766, 7767, 7768, 7778, 7779, 7780, 7781, 7783, 7784, 7786, 7788, 7789, 7790, 7795, 7796, 7797, 7798, 7801, 7802, 7803, 7814, 7816, 7825, 7828.	**N (CCT2)** = 93229896 **N_1 (CCT2 &&B/A $\pm$ 1.8 μs)** = 21785116 **N_2 (γ)** = 221256 **N_3 (n)** = 34103

Time and energy resolution

The time resolution is estimated by the peak width of prompt gamma-rays in the time-of-flight spectrum. In order to improve the time resolution, a correction was made using the dependence of the registration time on the pulse amplitude (slewing correction). As a result, the obtained time resolution of the time-of-flight spectrometer was σ_t = 117 – 121 ps at a threshold neutron energy of 1 MeV. This corresponds to the time resolution of the neutron detectors themselves $\sigma_t \approx$ 110 – 114 ps. The energy resolution of the spectrometer for neutron energy E is determined by the error in the flight distance σ_l and the time resolution σ_t and is calculated using the formula

$$\frac{\sigma_E}{E} = \gamma(\gamma+1)\left[\left(\frac{\sigma_l}{l}\right)^2 + \left(\frac{\sigma_t}{t}\right)^2\right]^{1/2}, \quad (3)$$

where γ is the gamma factor, l is the flight distance, t is the neutron flight time.

The obtained energy resolution for detectors ND2 – ND4, as a function of neutron energy, is shown in Fig. 5. At the maximum energy of the studied range of 200 MeV, it is ~18%.

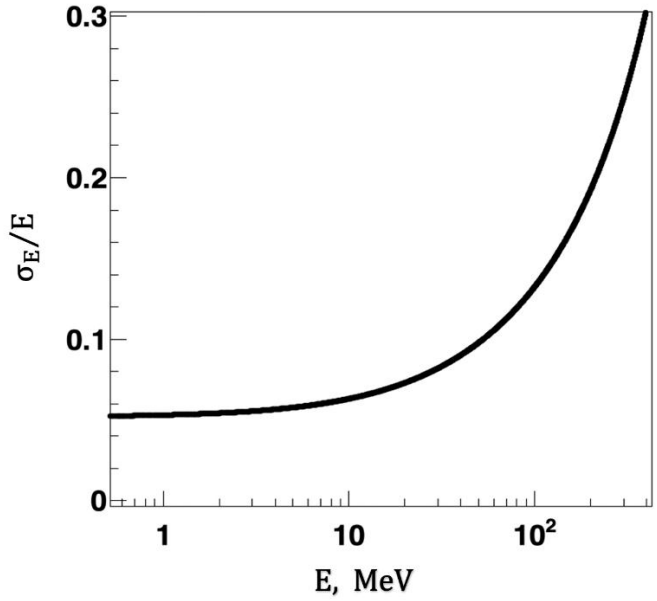

Fig. 5. Energy resolution at a flight distance of 30 cm for detectors ND2 – ND4.

Gamma-ray discrimination

To select events caused by neutrons, it is necessary to suppress background events associated with the registration of gamma quanta. For this purpose, the spectrometer uses the pulse shape discrimination (PSD) method. In our case, for the used registration channel with the TQDC16VS module, the best result is achieved with integration intervals of 120 ns and 1.5 μs for the fast component Qf_{ast} and the total pulse Q_{total}, respectively. To assess the quality of separation of events from neutrons and gamma quanta, it is customary to use the PSD parameter, calculated as

$$PSD = \frac{Q_{fast}}{Q_{total}} , \quad (4)$$

as well as the FOM (Figure of Merit) value, which numerically evaluates the quality of separation for a given energy and is defined as the ratio of the difference between the average values of the neutron peaks μ_n and gamma quanta μ_γ to the sum of their widths at half-maximum for the selected energy range (FWHM)

$$FOM = \frac{|\mu_\gamma - \mu_n|}{FWHM_\gamma + FWHM_n} . \quad (5)$$

As noted earlier, to eliminate the effect of pulse overlap, events with one incident beam ion are selected in the time interval of ± 1.5 μs (Before/After protection). The quality of *n/γ*-separation obtained is shown in Fig. 6.

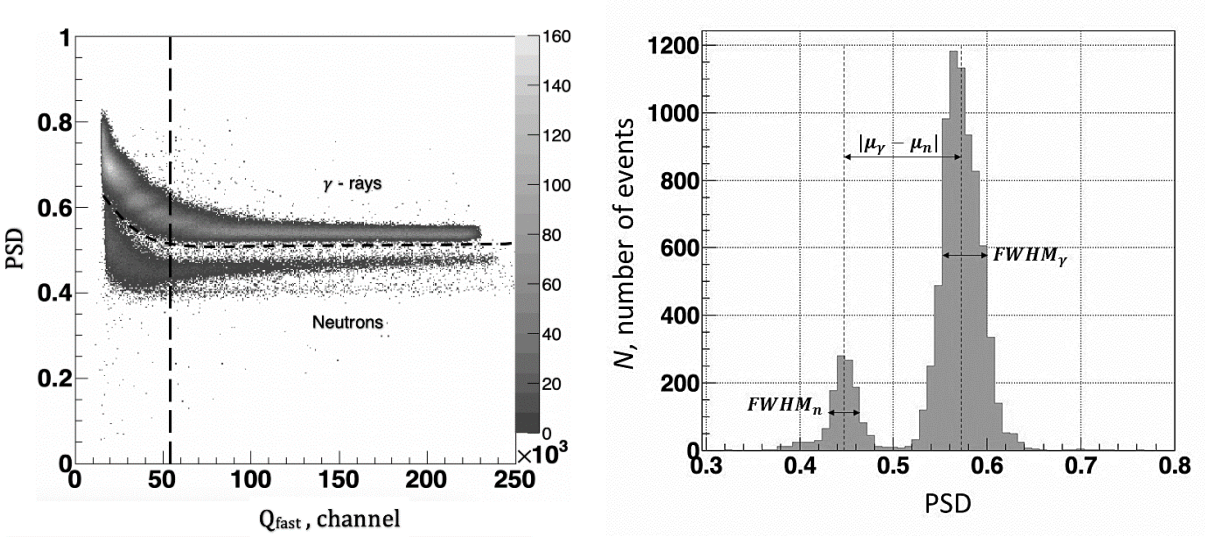

Fig. 6. Separation of events by pulse shape caused by neutrons and gamma quanta in the ND4 detector (left) and the quality of separation of events from neutrons and gamma quanta (right) at a Q_{fast} value corresponding to a neutron energy of 1 ± 0.1 MeV (shown by the dotted line in the left figure).

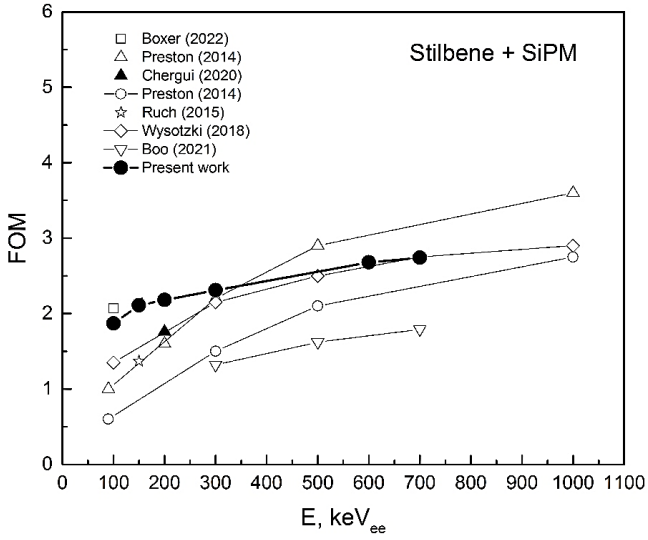

Fig. 7. Dependence of the FOM value on the amplitude expressed as the electron energy E_{ee}, obtained in this work and the works of other authors [26 – 31].

For the amplitude corresponding to the threshold energy of 1 MeV, the FOM value for the ND2 – ND4 detectors lies in the range of 2.17 – 2.47, and for the ND1 detector it is 1.98. In the low-amplitude region, the measured FOM values exceed the data of most groups [26–31] that studied the characteristics of stilbene- and SiPM-based neutron detectors as it is shown in Fig. 7.

The comparison of the time-of-flight spectrum of neutrons and the background of detected gamma quanta measured by the ND4 detector at an angle of 95^{o} is shown in Fig. 8.

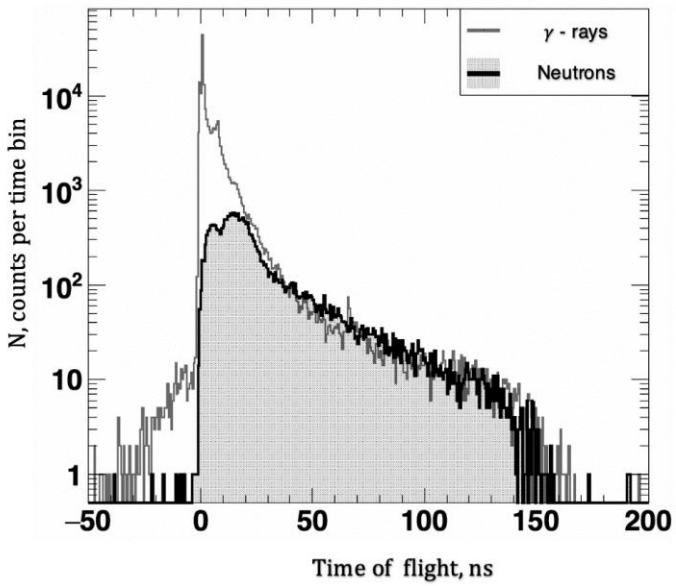

Fig. 8. Comparison of the time-of-flight spectrum of neutrons and the background of detected gamma quanta measured by the ND4 detector at an angle of 95°.

The background of gamma quanta is superimposed on the neutron spectrum, and its intensity significantly exceeds the number of neutron events. This demonstrates the importance of using the PSD method to isolate neutron events. In our case, the obtained high value of the FOM parameter allows us to almost completely suppress the background of gamma quanta, which proves the practical absence of the peak of prompt gamma quanta in the time-of-flight spectrum of neutrons.

TOF spectra and neutron background

The neutron background consists of two components of different origin. This is the background of random neutrons, which have a uniform distribution in time, and the background of secondary neutrons, correlated with the passage of beam ions through the experimental zone.

The second component, in turn, consists of neutrons from the interaction of ions with beam path materials and secondary neutrons caused by the interaction of particles generated in the target with surrounding materials.

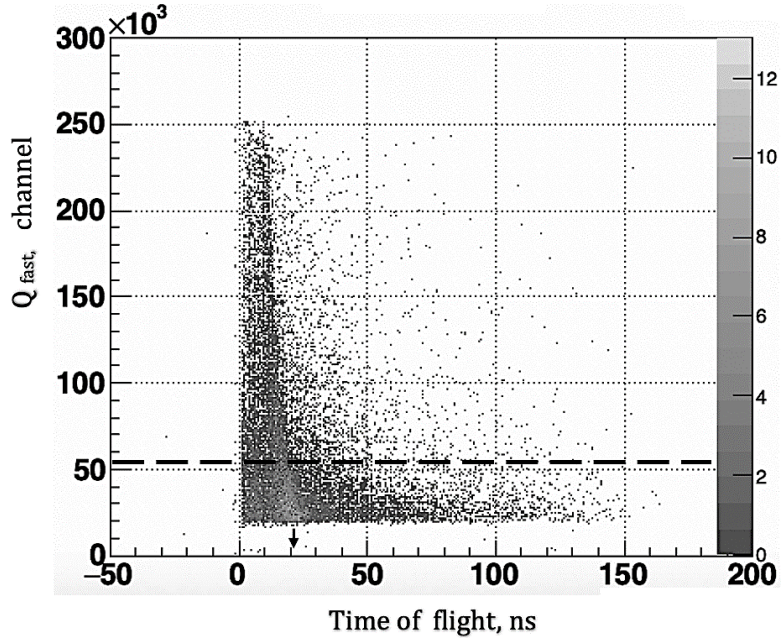

Fig. 9. Distribution of registered neutrons by the ND3 detector, where the horizontal scale is the time of flight, the vertical scale is the integral of the fast component of the pulse: the dotted line shows the threshold value of Q_{fast}, corresponding to a proton energy of 1 MeV, the arrow is the time of flight value for neutrons with an energy of 1 MeV.

The spectrometer detectors are located inside the large BM@N magnet of the setup, which affects the background conditions in a certain way. Measurements have shown that the background of random neutrons is practically absent in the time-of-flight spectra. This is clearly seen from the two-dimensional distribution of neutrons registered by the ND3 detector shown in Fig. 9, where the horizontal scale shows the time of flight, and the vertical scale shows the integral of the fast component of the pulse. It is seen that there are practically no background events both before the spectrum and at $t > 150$ ns.

The background from neutrons generated by the interaction of ions with beam path materials was studied in a target-free measurement. As can be seen from Fig.10, which shows the time-of-flight spectra of neutrons measured with and without a CsI target, the contribution of such neutrons is negligibly small and amounts to less than 1%.

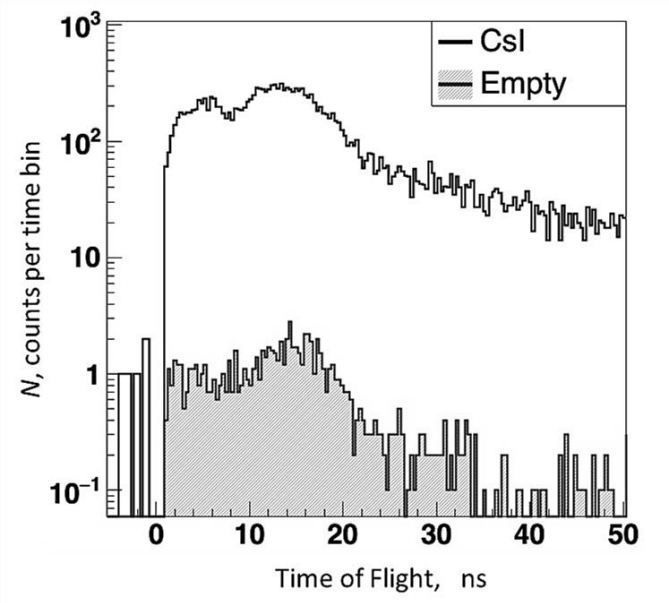

Fig. 10. Time-of-flight spectra of neutrons measured with the ND4 detector, with and without a CsI target.

The conducted studies have shown that the main source of background neutrons is the interaction of particles produced in the target with the surrounding materials – parts of the BD detector and other detectors of the BM@N facility, as well as magnet materials. Due to the limited space in which the spectrometer is located and the use of small flight distances, it is not possible to implement measurements with a shadow cone for experimental assessment of the magnitude of this background. Therefore, the contribution of such background neutrons to the measured time-of-flight spectrum was estimated by modeling using GEANT4. The DCM-QGSM-SMM code was used as a generator of nucleus-nucleus interaction events. Modeling showed that the greatest contribution in the short-time region is made by neutrons from the interaction of high-energy particles with the BD detector materials, while in the long-time region the contribution of background neutrons from interactions with the materials surrounding the spectrometer dominates.

The time-of-flight spectra of neutrons measured by the ND1 and ND4 detectors with a detection threshold of 1 MeV are shown in Fig. 11. The statistics of events shown were collected over four days of continuous measurements. The figure also shows the contributions of background neutrons estimated by modeling.

It should be noted that the high time resolution of the spectrometer and the use of short flight distances are important for minimizing the contribution of background neutrons and obtaining reliable measurement results. Therefore, it is important to emphasize that the compactness of the created neutron spectrometer is of fundamental importance.

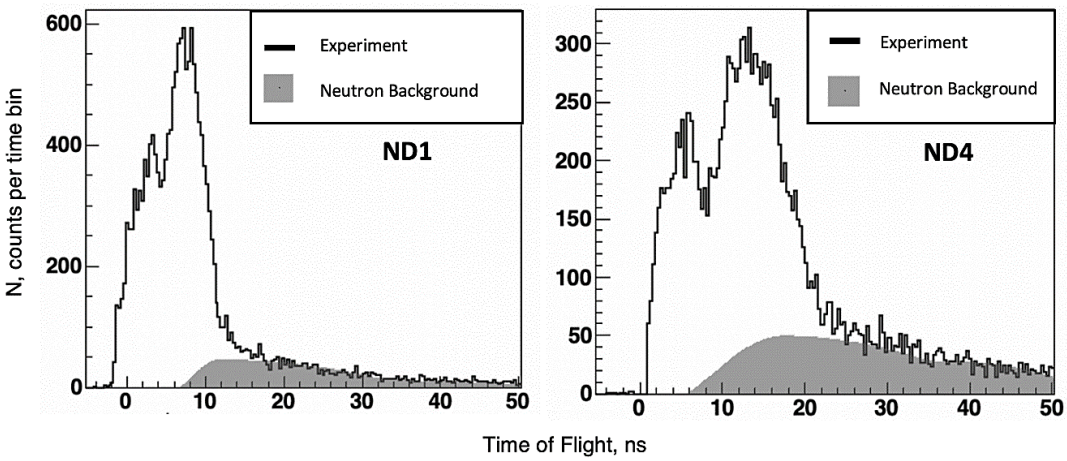

Fig. 11. Time-of-flight spectra of neutrons measured with detectors ND1 and ND4. Dark areas show the contribution of background neutron

4. Analysis of the collision centrality and the trigger efficiency

The important issue is determination of centrality interval of the triggered Xe + CsI collisions in the experiment. For this aim we used MC simulation with code DCM-QGSM-SMM + GEANT4 of the Barrel Detector response for collisions with different values of the impact parameter as it is shown in Fig. 12. The result of simulation of the multiplicity of fired channels well reproduces of the experimental distribution shown in Fig. 13a which ratio is close to unit (see Fig. 13b).

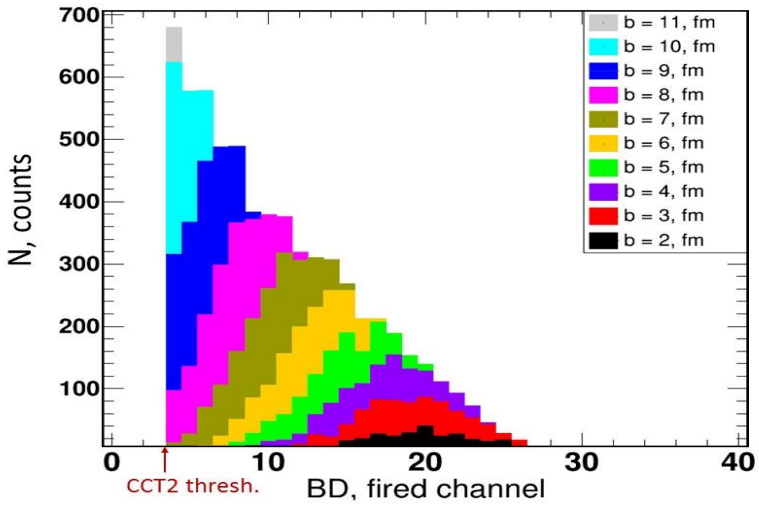

Fig. 12. Simulation of the Barrel Detector response at different impact parameters.

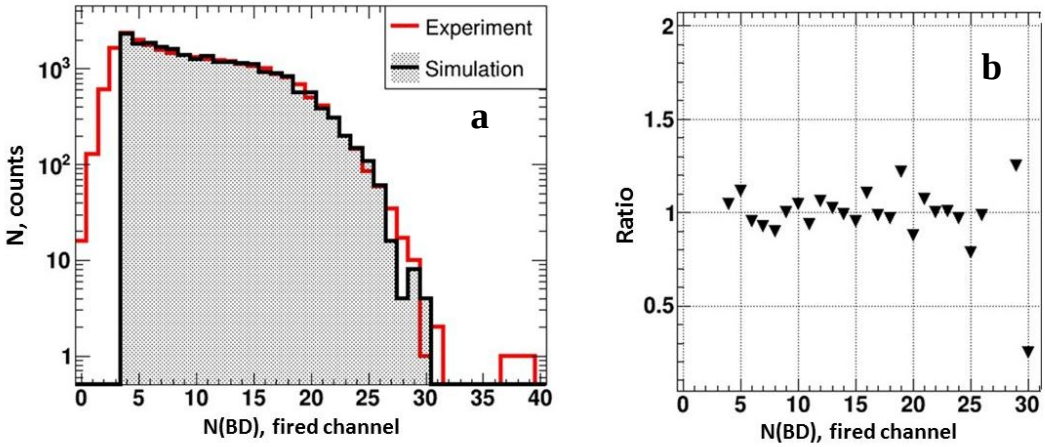

Fig. 13. A comparison of the BD fired channel distribution simulated with the experimental distribution (a) and the ratio of experiment to simulation (b).

As a result, we obtained the efficiency of triggering Xe + CsI collisions for CCT2 trigger with N(BD) > 3. In the Fig. 14a one can see the probability of nuclear interactions with impact parameter. The probability rapidly falls down when we come to the peripheral region and at b = 14 fm only 1% of Xe ions interact with target nucleus. The trigger efficiency as a function of impact parameter found from the simulation results is shown in Fig. 14b. It is clearly seen that the interaction trigger CCT2 effectively selects the collisions with centrality of 0 – 60%.

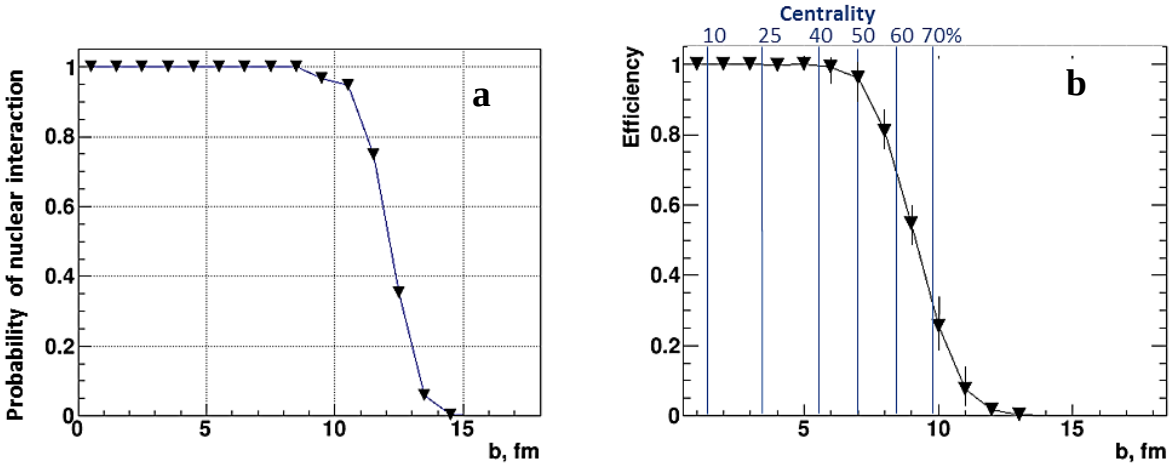

Fig. 14. the probability of nuclear interactions with impact parameter (a) and the trigger efficiency as a function of impact parameter (b).

5. Energy spectra of neutrons

The energy spectra of neutrons are double differential cross sections of neutron production and are obtained after subtracting the background of secondary neutrons using the expression

$$\frac{d^2\sigma}{dEd\Omega} = \frac{\Delta N}{\Delta E \cdot \Delta\Omega \cdot \varepsilon(E) \cdot n \cdot I \cdot k_1 \cdot k_2} \quad , \qquad (6)$$

where ΔN is the number of events in the energy range ΔE, $\Delta\Omega$ – the solid angle, $\varepsilon(E)$ – the detector efficiency at neutron energy E, n – the number of target nuclei per 1 cm^2, I – the number of beam ions per target, k_1 – the correction for the dead time of the spectrometer, and k_2 – the correction taking into account the selection of events with one incident beam ion in a time interval of ± 1.5 μs.

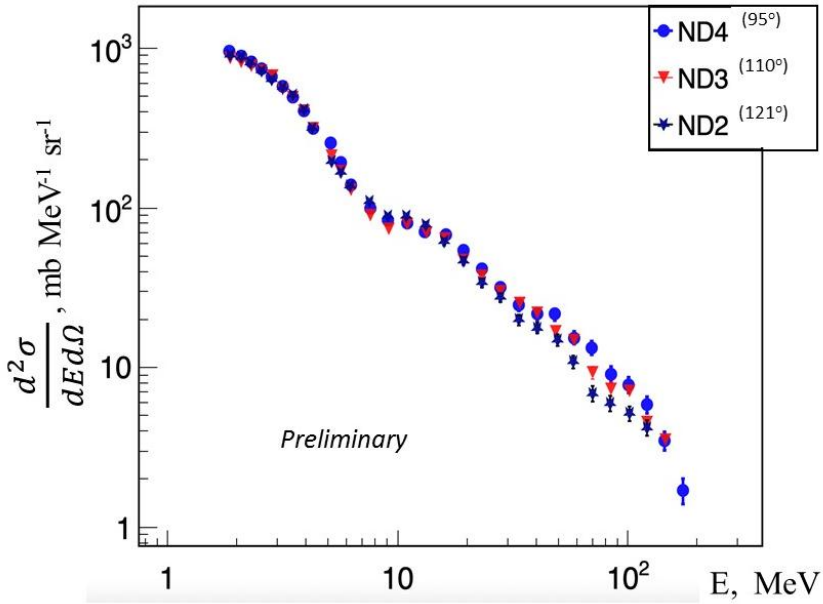

Fig. 15. Energy spectra of neutrons at angles of 95°, 110° and 121°, measured by detectors ND1 – ND4.

The results of measurements of the neutron energy spectra at different angles with the detectors ND1 – ND4 are shown in Fig.15. As can be seen from the figure, the obtained spectra are in good agreement in the low energy region.

The difference becomes noticeable with increasing neutron energy in the region above 20 MeV. This shows that in the low energy region the angular distribution of neutrons is close to isotropic, and therefore the velocity of the target nucleus residual emitting such neutrons is small in lab. frame.

Here it is important to note that the neutron spectra were obtained in centrality interval from central to a part of peripheral collisions (see the trigger efficiency in Fig. 14b).

6. Data analysis with the Moving Source Model

The experimental energy spectra of neutrons were analyzed in framework of three moving source model (MSM). The first source S1 reproduces the hard part of the spectra and other sources S2 and S3 describe the neutron emission in fragmentation decay and evaporation process respectively. The model applies the Maxwell-Boltzmann distribution to describe energy dependence of the neutron production cross section and assumes the isotropic emission of the neutrons in the frame of emitting source. The energy spectrum of the neutrons emitted at the angle θ with the kinetic energy E is derived from the Lorenz transformation to the laboratory frame. For the three neutron sources the energy spectrum is given by

$$\frac{d^2\sigma}{dEd\Omega} = \sum_{i=1}^{3} pA_i \, exp\{ - (\frac{E+m-p\beta_i \cos\theta}{(1-\beta_i^2)^{1/2}} - m)/T_i\}, \qquad (7)$$

where the neutron momentum $p = (E^2 + 2Em)^{1/2}$, m is the rest mass of a neutron and A_i, T_i, β_i are the parameters of amplitude, slope temperature and longitudinal velocity of the sources.

The result of the MSM fitting is shown in Fig. 16 for angles 95^o and 121^o together with contributions of the sources S2 and S3. The velocities of these sources are closed to zero, that means the isotropic emission of neutrons from these sources in the Lab. Frame. The obtained parameter values are given in Table 2.

Table 2. The obtained values of MSM parameters.

Source	A_i	T_i (MeV)	β_i
S1	0.252	40	0.10
S2	1.8	7.3	~0
S3	78.8	1.2	~0

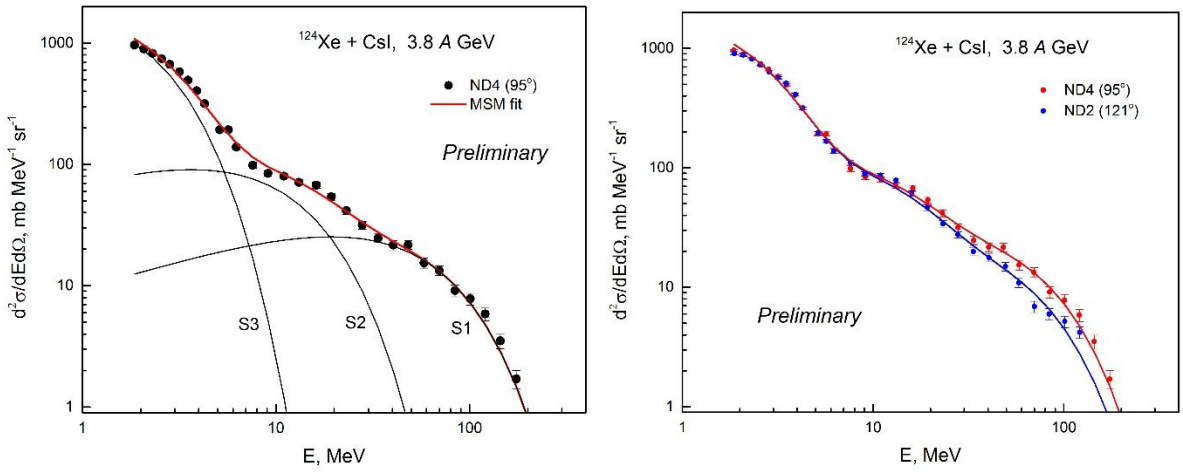

Fig. 16. The result of MSM fitting of experimental neutron spectra obtained at angles 95° and 121°: the points – the experimental data, the lines – the MSM fit.

7. Comparison with prediction of DCM-QGSM-SMM code

The experimental neutron spectra are compared with prediction of DCM-QGSM-SMM code in Fig. 17.

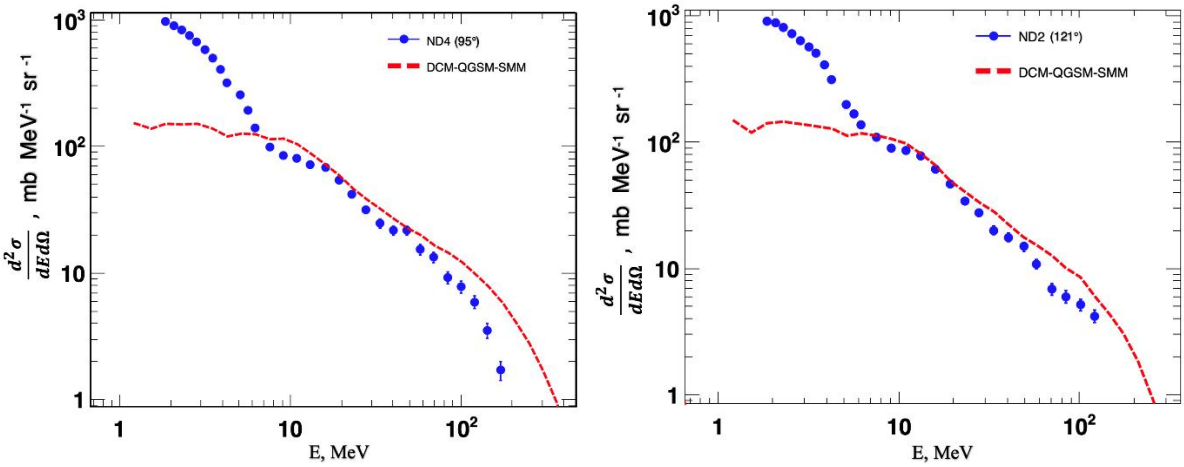

Fig. 17. A comparison of experimental data with prediction of the DCM-QGSM-SMM code.

It is clearly seen that in a region above ~8 MeV the code is slightly overestimates the neutron emission but at lower energies it gives much smaller the neutron yield. It seems that the present code version does not include the neutron emission by evaporation process from excited fragments of target spectators.

A comparison with predictions of other theoretical models is in progress.

8. Spectrometer upgrade for next BM@N runs

New spectrometer mechanics has been developed. A photo of the new spectrometer setup is shown in Fig. 18. The new setup allows more precise installation of the detectors with a definite flight path and an angle.

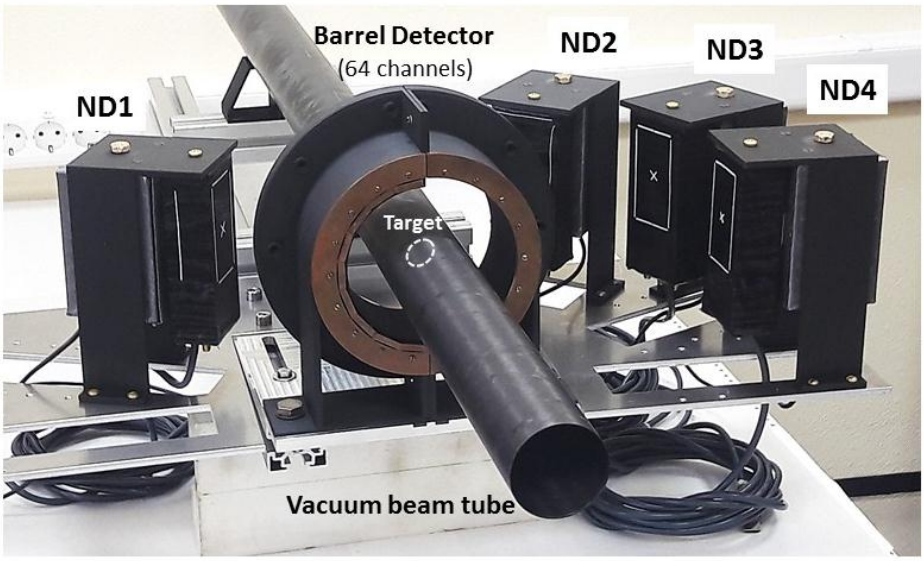

Fig. 18. A photo of new spectrometer setup (prototype).

Next extension of neutron measurements at BM@N experiment is study of neutron energy spectra at small angles to the beam direction. Besides a scientific interest the result can be useful as reference data for the HGND project and study of energy and angular distributions of neutrons coming to nZDC (FHCal). New neutron detectors have been developed with stilbene and PMT Hamamatsu R2490-07 and overlap an energy range above 100 MeV. A list of the detectors is given in Table 2 and a scheme and photo of the detector is shown in Fig. 19. In this measurement the flight path is 360 cm and event statistics required is obtained rather fast, not more of one day of measurements (with and without target).

All the detector can be fast installed and dismounted. The events induced by charged particles are discriminated with a scintillation veto-detector VD with 5- mm plastic scintillator and readout by two SiPMs.

Table 2. A list of the detectors developed for measurements at small angles.

Detector	Stilbene	Angle
ND1	D31 × 31 mm^3	0^o
ND2	D31 × 31 mm^3	3^o
ND3	D40 × 20 mm^3	7^o
ND4	D40 × 20 mm^3	12^o

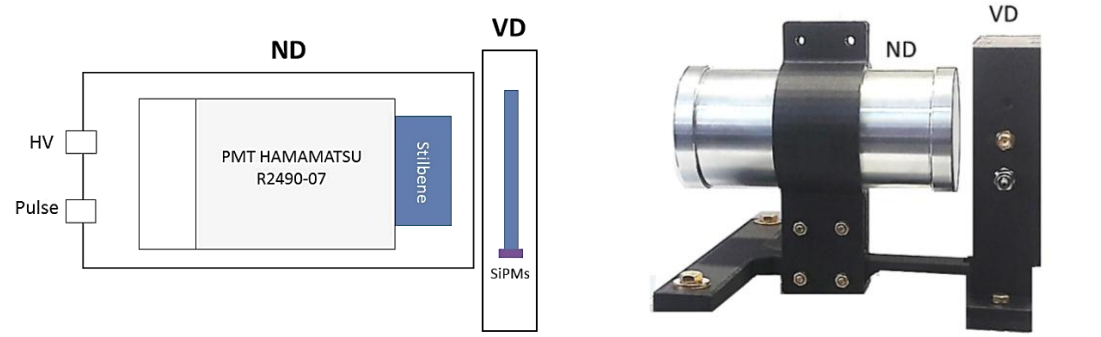

Fig. 19. A scheme and photo of the new neutron detector with stilbene and PMT.

9. Conclusion

A compact time-of-flight neutron spectrometer has been developed as a part of the BM@N setup for measuring neutron energy spectra in the energy range of 1–200 MeV at large angles to the direction of the heavy ion beam. The spectrometer uses stilbene-based neutron detectors coupled to an assembly of four SiPMs with time resolution of $\sigma_t \approx 112 \pm 2$ ps that allows to perform neutron measurements in a wide energy range at short flight distances of several tens centimeters. In comparison with traditional time-of-flight spectrometers using flight distances of several meters, the developed table-scale spectrometer offers a high rate of event statistics collection at a significantly lower background level of secondary neutrons. The use of the n/γ-pulse shape discrimination method in the spectrometer with a FOM factor of > 2 provides almost complete suppression of the gamma-quantum background and ensures reliable detection of neutron events.

The experiment performed to measure double differential cross-sections of neutron production in Xe + CsI collisions at an energy of 3.8 *A* GeV on the BM@N setup channel has

proven that the compact spectrometer created fully meets the requirements imposed on it. In the future, it is planned to use the spectrometer as part of the BM@N setup to study neutron emission in nucleus-nucleus collisions on beams of various nuclei with energies from 2 to 4 *A* GeV.

References

1. R. Madey, W.-M. Zhang, B. D. Anderson et al., Phys. Rev. C, V.42 (1990) 1068.
2. W. M. Zhang, R. Madey, J. Schambach et al., arXiv:nucl-ex/9510001v1 3 Oct 1995.
3. A. R. Baldwin, R. Madey, W.-M. Zhang, et al., Phys. Rev. C, V.46 (1992) 258.
4. M. Pachr, M. Sumbera, A. Kugler, et al., Acta Physica Slovaca V.44 (1994) 35.
5. P. Pawłowski et al., Phys. Rev. C, V.108 (2023) 044610.
6. A. Kugler, V. Wagner, M. Pachr, et al., Phys. Lett. B, V.335 (1994) 319.
7. W. Trautmann (for the ALADIN/LAND collaboration), Formation and Decay of Equilibrated Spectator Nuclei at Relativistic Bombarding Energies
8. D. Satoh, D. Moriguchi, T. Kajimoto, et al., Journal of the Korean Physical Society, Vol. 59 (2011) p. 1741.
9. D.-H. Moon, C. Ham, E. In, et al., Neutron production double differential cross section from Carbon, Niobium and Bismuth targets bombarded by 290 MeV/u 136Xe ions, 15th International Conference on Nuclear Data for Science and Technology (ND2022), 2022.07.
10. V. I. Yurevich, R.M. Yakovlev, V. G. Lyapin, Physics of Atomic Nuclei, V. 75 (2012) 192.
11. T.A. Armstrong, K.N. Barish, S. Batsouli, et al., Measurements of Neutrons in 11.5 A GeV/c Au + Pb Heavy-Ion Collisions, arXiv:nucl-ex/9909001v1 2 Sep 1999.
12. H. Appelshäuser, J. Bächler, S.J. Bailey, et al., Eur. Phys. J. A, V.2 (1998) 383.
13. ALICE Collaboration, Data-driven model for the emission of spectator nucleons as a function of centrality in Pb-Pb collisions at LHC energies, CERN Report ALICE-PUBLIC-2020-001, 2020.
14. S. Afanasiev et al. (BM@N Collaboration), The BM@N spectrometer at the NICA accelerator complex, arXiv:2312.17573v2 [hep-ex] 11 Mar 2024.
15. https://afi.jinr.ru/TDC
16. A.D. Carlson, V.G. Pronyaev, R. Capote et al., Nuclear Data Sheets, V.148, 143-188 (2018).
17. S. Chiba, S. Morioka, T. Fukahori, J. Nucl. Sci. and Techn., 33 (1996) 654.

18. M. Harada, Y. Watanabe, S. Chiba, T. Fukahori, J. Nucl. Sci. and Techn., 34 (1997) 116.
19. L.M. Kerby, S.G. Mashnik, arXiv:1505.00842v1 [nucl-th] 4 May 2015.
20. M. Yuly, T. Eckert, G. Hartshaw, et al., Phys. Rev. C97 (2018) 024613.
21. A. Di Chicco, Characterization of a stilbene organic scintillator for use as a broadband neutron spectrometer in mixed radiations fields, PhD Thesis, Soutenue à Aix-Marseille Université, 2022.
22. А.Д. Кириллов, В.Г. Ляпин, П.А. Рукояткин и др., Сообщение ОИЯИ Р13-90-193, 1990.
23. S.D. Howe et al., NIM in Phys. Res., 227 (1984) 565.
24. J.L. Fowler, J.A. Cookson, M. Hussain, et al. NIM 175 (1980) 449.
25. A.R. Garcia, E. Mendoza, D. Cano-Ott, et al., NIM in Phys. Res., A868 (2017) 73.
26. B. Boxer, B. Godfrey, C. Grace et al., arXiv:2209.13979v2 [physics.ins-det] 21 Dec 2022, Journal of Instrumentation, V. 18 (2023).
27. A. C. Chergui, E. V. Popova, A. A. Stifutkin, et al., ICNRP Volga 2020; J. Phys.: Conf. Ser. 1689 (2020) 012039.
28. M. Preston, J. E. Eberhardt, and J. R. Tickner, IEEE Transactions on Nuclear Science, V.61 (2014) 2410-2418.
29. M. Ruch, M. Flaska, S. A. Pozzi, Nuclear Instruments and Methods in Physics Research Section A 793 (2015).
30. C. Wysotzki, Master's thesis, March 2018, Physikalischen Institut B, Aachen.
31. J. Boo, M. D. Hammig and M. Jeong, Scientific Reports (2021) 11:3826.